ELSEVIER

Journal of Molecular Catalysis A: Chemical 162 (2000) 317–334

JOURNAL OF MOLECULAR CATALYSIS A: CHEMICAL

www.elsevier.com/locate/molcata

On the role of hydrogen during the reduction–carburation of MoO_3 into molybdenum oxycarbide

Christophe Bouchy [a,b], Cuong Pham-huu [a], Marc J. Ledoux [a,*]

[a] *Laboratoire de Chimie des Matériaux Catalytiques, GMI-IPCMS-ECPM, Université Louis Pasteur, Strasbourg 25, rue Becquerel, 67087 Strasbourg Cedex 2, France*

[b] *Leverhulme Centre for Innovative Catalysis, Department of Chemistry, Liverpool L69 3BX, UK*

Abstract

The presence of hydrogen is necessary to form the oxycarbide ($MoO_{2.4}C_{0.2}H_{0.8}$) from MoO_3. This hydrogen should be dissociated either by traces of MoO_2 or Pt in order to form a bronze, the precursor of the oxycarbide. This mechanism induces a topotactic formation of the new material, the (200) oxycarbide planes being parallel to the initial $(0k0)$ planes of MoO_3. In the absence of hydrogen only non-topotactic formation of MoO_2 is observed.

Keywords: Hydrogen; Reduction–carburation; Molybdenum oxycarbide

1. Introduction

The selective isomerization of long paraffin chains is an industrially important reaction, for increasing the octane number (C_4–C_{10} range) or decreasing the freezing point of gas–oil and lubricant ($> C_{10}$ range) [1–5]. Up to now, commercial catalysts for this reaction are bifunctional, based on platinum dispersed on acidic materials, i.e. chlorinated alumina or zeolite. For alkane molecules containing more than six carbon atoms, the maximum isomerization selectivity of these catalysts can only be reached at a low conversion level, inducing a significant decrease in yield [6,7]. Moreover, this loss increases with the carbon number of the aliphatic molecule [8].

During the last decade, work from Ledoux et al. [9–14] have shown that a molybdenum oxycarbide, namely MoO_xC_y, exhibits high isomerization yield for C_4–C_{16} hydrocarbon range, for example 80% isomerization yield with *n*-C_{16} [14]. This phase consists of a fcc structure ($a_{cub} = 4.10$ Å) with a high over-stoichiometry of heteroatoms (C, H, O) compared to the metal [15]. This oxycarbide is synthesized by reduction–carburation of MoO_3 under hydrogen–hydrocarbon flow at 350°C, the overall working pressure being in the 1–20 bars range [11]. It should be noticed that when bulk MoO_3 is used as precursor, the MoO_2 sub-oxide is also formed in addition to the oxycarbide. The MoO_2 formation seems to follow a different pathway than the oxycarbide [12,16].

* Corresponding author. Tel.: +33-3-88-13-68-81; fax: +33-3-88-13-68-80.

E-mail address: ledoux@cournot.u-strasbg.fr (M.J. Ledoux).

1381-1169/00/$ - see front matter
PII: S1381-1169(00)00300-9

Previously, Lee et al. [17] reported the formation of a molybdenum oxycarbide phase during the reduction–carburation of Pt (0.25 wt.%)/MoO_3 by an hydrogen–methane mixture. As molybdenum bronzes H_xMoO_3 can be formed at room temperature by hydrogen spillover on Pt/MoO_3, this result suggested that the true precursor of the oxycarbide was a molybdenum bronze. Moreover, a pure oxycarbide phase was obtained from a bronze precursor, and no MoO_2 formation was detected. Choi et al. [18] and Jaggers et al. [19] reported a similar phenomenon for molybdenum oxynitride synthesis.

The aim of this work is to understand the role of hydrogen in the formation of the molybdenum oxycarbide during the 350°C isothermal reduction–carburation of MoO_3. For this purpose, using pure MoO_3 or MoO_3 impregnated with Pt traces will be proved to be of interest. The activation of MoO_3 under different conditions will be achieved, and characterization of the solid during and/or after synthesis will be carried out using different techniques.

2. Experimental section

2.1. Precursors

Strem Chemicals commercially supplied MoO_3 (purity 99.95%) was used. This oxide, crystallizing in an orthorhombic system, exhibits a strong anisotropy, i.e. platelet form, and lamelar structure made of layers of MoO_6 octahedra linked by van der Waals forces. The specific surface area was equal to 0.6 $m^2\ g^{-1}$. Before activation and catalytic test, the oxide was calcined for 12 h at 700°C, to increase the anisotropy of the particles [20]. The calcined oxide will be designated as Mo-700. The specific surface of the oxide after calcination remained unchanged.

For platinum impregnation, molybdenum oxide was first impregnated with an aqueous solution of $(NH_4)_xPtCl_2$ (Strem Chemicals) using the pore volume method. The solid was then dried for 4 h at 110°C and calcined for 2 h at 400°C. After calcination, the platinum concentration calculated from atomic adsorption analysis was equal to 0.25 wt.%. This sample will be named Mo–Pt.

2.2. Activation process

The MoO_3, either calcined at 700°C or doped with platinum, was activated with an hydrogen–*n*-heptane mixture at 7 bar and at 350°C. Details concerning activation protocol, catalytic microreactor and product detection have been published elsewhere [10,11]. Activation and catalytic test conditions were typically: 0.3 g precursor, 200 ml min^{-1} gaseous hydrogen flow, $H_2/n\text{-}C_7H_{16} = 30$. *n*-Heptane conversion as well as cracking and isomerization selectivity were calculated on a carbon basis.

Commercial MoO_3 was also activated by an helium–*n*-heptane mixture at 7 bar and at 350°C. Experimental conditions were the same as previously, except that hydrogen flow was replaced by an equivalent helium flow.

In a last experiment, commercial MoO_3 was reduced under pure hydrogen at 350°C and at 1 bar.

2.3. Characterization techniques

X-ray powder diffraction (XRD) was used for structural characterization of the samples. XRD measurements were performed on a Siemens Model D-5000 diffractometer working in the $\theta/2\theta$ mode, with Cu K_α monochromatic radiation ($\lambda = 1.50901$ Å). Each sample, either crushed or not, was deposited on the sample holder under dry nitrogen in order to minimize the air pollution, and the powder was packed into 0.5 mm depressions in 40×44 mm polymer slides. Samples were exposed to radiation from 10 to 80 (2θ angle) with a step scan mode of 2θ step = 0.02 and a 10-s step time. The nature of the different crystalline phases was checked using the database of the Joint Committee on Powder Diffraction Standard (JCPDS). Mean crystallite sizes were determined using the Scherrer equation with the normal assumption of spherical crystallites.

The specific surface area (Sg) was obtained from nitrogen physisorption at LN_2 (77 K) using a Coulter AS 3100 sorptometer. The measurements were made at liquid nitrogen temperature with nitrogen (Air Liquide, 99.95%) as the adsorbate gas. The porosimeter allowed the measurement of different kinds of surface area contributions: S_{BET} is the surface area calculated from a nitrogen isotherm using

the BET method, and $S_{micropore}$ is the surface area of the micropores calculated by applying the *t*-plot method developed by de Boer [21].

Transmission Electron Microscopy (TEM) was used to characterize the microstructure of the material. The HRTEM experiments were carried out with a Topcon EM-002 B microscope working at 200 kV equipped with a Kevex analytical system allowing the detection of light elements. The high-resolution objective lens, with a spherical aberration coefficient (Cs) of 0.5 mm, allowed a point-to-point resolution of 0.17 nm. Samples were supported on holey carbon-coated copper grids by simply grinding the specimen between glass plates and bringing the powder in contact with the grid. To prevent artifacts due to contamination, no solvent was used at any stage of the preparation. Great care was taken during HRTEM experiments in order to avoid heating effects from the electron beam.

Elemental analysis was carried out by absorption spectroscopy at the Service Central d'Analyses of the CNRS (France).

3. Results

3.1. Characteristics of the precursors

XRD patterns of Mo-700 and Mo–Pt are displayed in Fig. 1. For each sample, the platelet-like shape of the oxide particles induces an abnormally high intensity of the $(0k0)$ diffraction plans associated to the basal planes of the platelet form of MoO_3. For Mo-700, the effect was even more pronounced as the anisotropy was increased by the calcination at 700°C. The XRD pattern of Mo–Pt is identical to the commercial oxide XRD pattern, and no platinum diffraction peaks were observed.

The initial specific surface area of both samples was very low, i.e. 0.2 $m^2\ g^{-1}$ for Mo-700 and 0.6 $m^2\ g^{-1}$ for Mo–Pt.

3.2. Catalytic results and catalyst characterization

3.2.1. Catalytic results

The evolution of the *n*-heptane conversion and of the *iso*-heptanes selectivity with time on stream for Mo-700 and Mo–Pt are presented in Fig. 2. As expected, no conversion was observed at the beginning of the test, as MoO_3 is inactive for isomerization [22]. The time needed to reach the steady state corresponded to the complete formation of the active phase, and is called the activation period. One should note that with platinum, the activation period was strongly shortened, i.e. 2.5 h instead of 10 h for the Mo-700 precursor.

For both systems, the steady-state conversion and selectivity were relatively close. This meant that the same kind of active sites seemed to have been generated, regardless of the precursor. Both solids exhibited good isomerization properties, as the isomerization selectivity was about 80–85% at 70% conversion. No deactivation was observed because

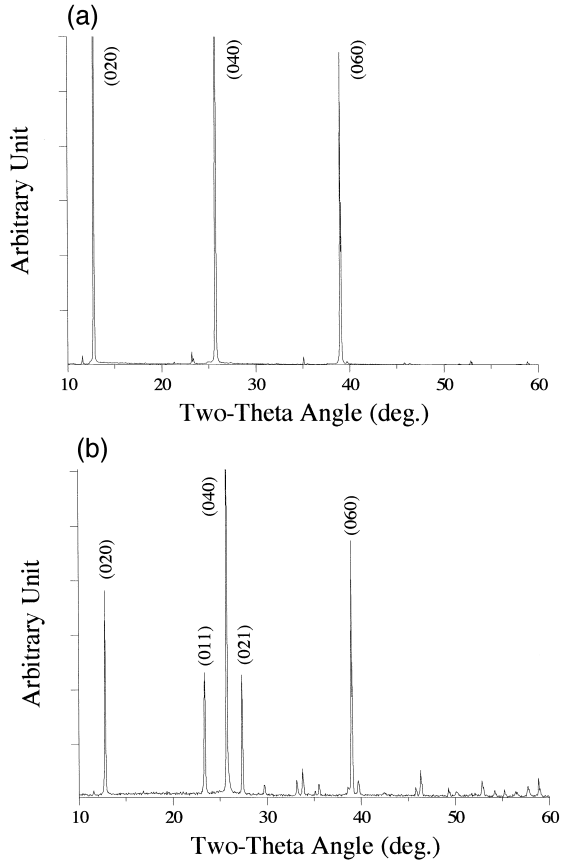

Fig. 1. XRD patterns of $MoO1_3$ (a) calcined at 700°C for 12 h, (b) doped with 0.25 wt.% Pt and calcined at 400°C. The 700°C calcination further increases particle anisotropy.

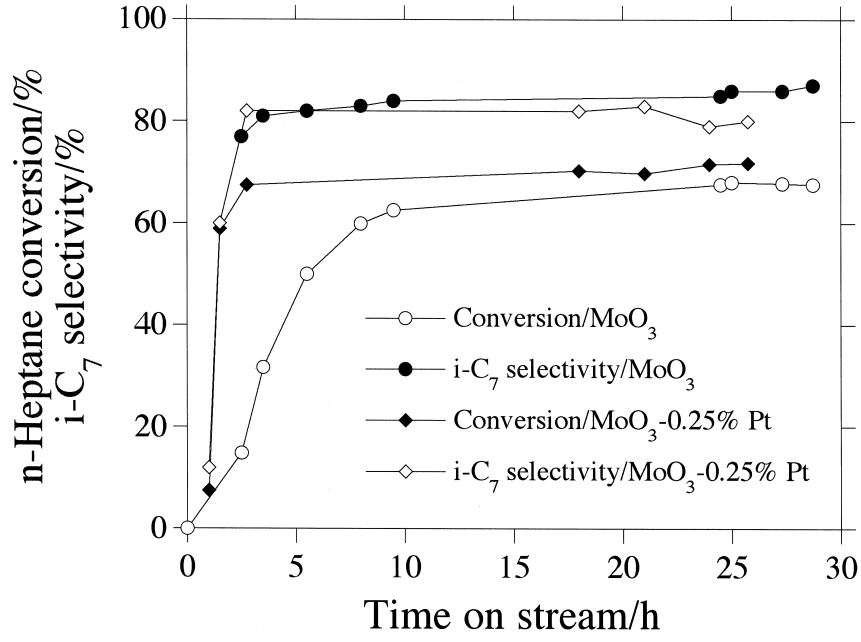

Fig. 2. *n*-Heptane isomerization, conversion and selectivity as a function of time on stream for Mo-700 and Mo–Pt.

no coke deposition occurred under these working conditions [23].

3.2.2. Catalyst characterization

3.2.2.1. Mo-700 precursor. The solid was characterized after 3 and 24 h time on stream. Each time corresponded, respectively, to the beginning and the end of the activation period (steady state).

SEM photographs of the solid after different activation time are shown in Fig. 3. Retention of the platelet shape of the solid particles during the transformation indicated that the overall process was pseudomorphic.

XRD characterizations of the product (ground and unground) after 3 and 24 h was also performed (Fig. 4). After 3 h, the sample contains no MoO_3 and two different crystalline phases have appeared. The first one is MoO_2 [24] and the second is not listed in the JCPDS files. This compound, called Mo-700-3 h, exhibits three different diffraction peaks corresponding to interplanar distances of 6.20, 3.05 and 2.05 Å. After 24 h, the final oxycarbide phase is formed at the expense of Mo-700-3 h and the XRD pattern remains the same for longer time on stream. The three diffraction peaks of the oxycarbide ($2\theta = 38.00$, 44.20 and 64.20) corresponded to the (111), (200) and (220) planes of the fcc structure ($a_{cub} = 4.10$ Å) [15]. Unlike MoO_2, the oxycarbide XRD pattern was strongly influenced by grinding the sample (Table 1). In particular, the relative intensity of the (111) and (220) planes, compared to the (200) plane, strongly increased after grinding. Similar results have also been reported by Volpe [34] during TPR synthesis of molybdenum nitride and carbide from MoO_3.

The abnormally high relative intensity corresponding to the (200) oxycarbide plane before grinding meant that these planes were basal planes of the platelets and their crystallographic orientation was the same as the initial $(0k0)$ MoO_3 planes. Indeed, the MoO_3–oxycarbide transformation appeared to be topotactic according to the Oswald and Gunter [25] definition. Interestingly, this was not the case for MoO_2, as grinding does not influence the sub-oxide diffraction patterns (Table 1).

TEM characterisation of the catalyst after 24 h on stream also confirmed the presence of MoO_2 and of

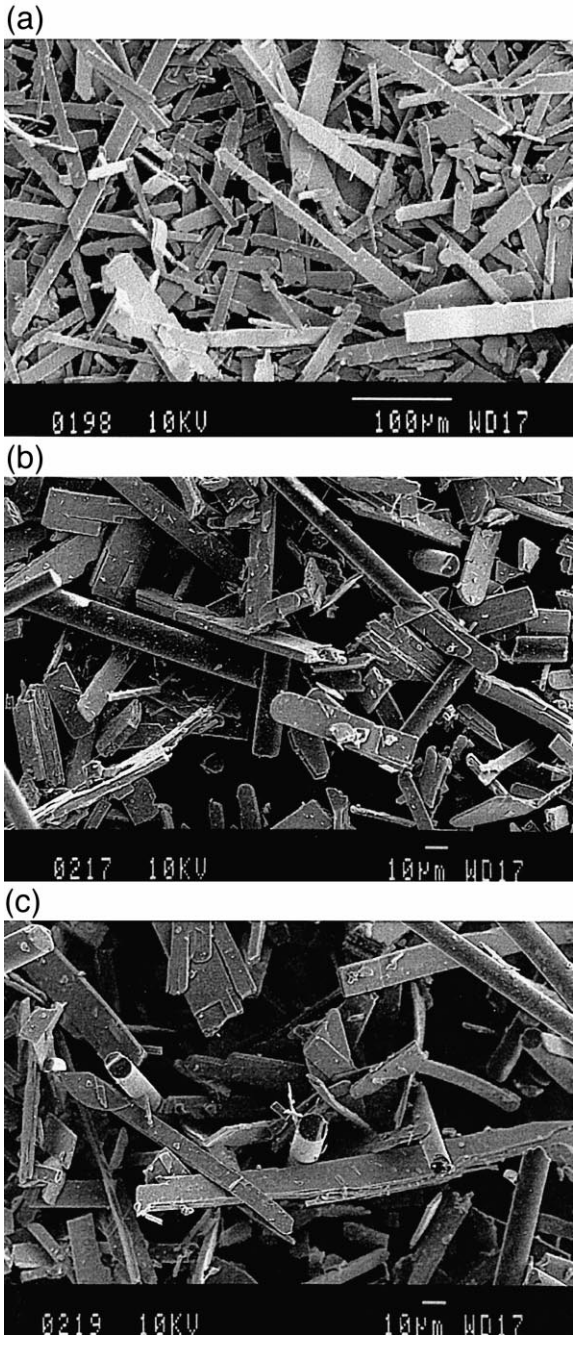

Fig. 3. SEM characterization of Mo-700 (a) before activation, (b) after 3 h and (c) after 24 h activation. For (b) and (c), rod-shaped particles are pure silica wool.

the oxycarbide (Fig. 5). MoO_2 particles were well crystallised and exhibited random orientation, as expected for a non-topotactic process. On the contrary, molybdenum oxycarbide showed a completely different morphology. The phase appeared much less crystallized and a selected area diffraction pattern (SADP) indicated that all the particles were oriented in the same direction, as a direct consequence of the topotactic process. The square symmetry of the diffraction pattern showed that crystallites were exposed to the [001] zone axis; the distance measured corresponding to (200) (2.05 Å) and (220) (1.18 Å) reflections. Furthermore, the size and the star-shape of the central spot strongly suggest the presence of (100) and (101) reflections. As odd reflections are forbidden for a perfect fcc structure, this implied that the metallic sites of the structure were not equivalent, probably because of the presence of metallic vacancies [15]. The stoichiometric formula of the oxycarbide was estimated by TPO and elemental analysis to be $MoO_{2.42}C_{0.23}H_{0.78}$. The oxygen content was probably overestimated because of sample passivation.

During the activation period, Mo-700 developed a significant specific surface area. After 3 h, S_{BET} was equal to 42 $m^2\ g^{-1}$ and increased to 64 $m^2\ g^{-1}$ after 24 h. This oxycarbide formation was also accompanied by the development of microporosity in the solid (Fig. 6). The micropore area represented about 75% of the overall area after 24 h. As the BET theory is not valid for microporous compounds, it should be stressed that the absolute S_{BET} value was meaningless. Moreover, the sample was passivated before measurement because of its high pyrophoricity and it is well known that passivation induces significant loss of surface area [19,26].

3.2.2.2. Mo–Pt precursor. As the activation period was very short, the catalyst was only characterized at steady state, i.e. after 24 h on stream.

The XRD patterns of the solid after 24 h of reaction are presented in Fig. 7. The very high background compared to the diffraction peaks detected implied that the solid crystallinity was very poor. The presence of platinum inhibited the MoO_2 formation and only four diffraction peaks were detected. These peaks were attributed to (111) and (200), (220) and (311) diffraction planes for a poorly crystallized fcc molybdenum oxycarbide. Interestingly, the crystallographic parameter (a_{cub} = 4.18 Å)

was slightly different to the one for the oxycarbide obtained without platinum (a_{cub} = 4.10 Å). This suggested that this oxycarbidic phase, synthesized in the presence of platinum, was identical to the one previously synthesized by Lee et al. [17], as the XRD characteristics of the two compounds are very similar. The stoichiometric formula of the oxycarbide was estimated to be $MoO_{0.95}C_{0.49}H_{0.78}$ by elemental analysis.

According to TEM (Fig. 8), the catalyst microstructure could be described as an amorphous phase with short-range order, similar to the oxycarbide synthesized without platinum. The HRTEM picture evidenced the presence of crystallised nodules with a 2.1 ± 0.1 Å interplanar distance ((200) plane). No MoO_2 particles were detected within the solid, which was consistent with the XRD result.

As with the Mo-700 precursor, the reduction–carburation was accompanied by a high development of specific surface area and microporosity. After 24 h, S_{BET} was found equal to 91 $m^2\ g^{-1}$ with a microporosity contribution as high as 84%.

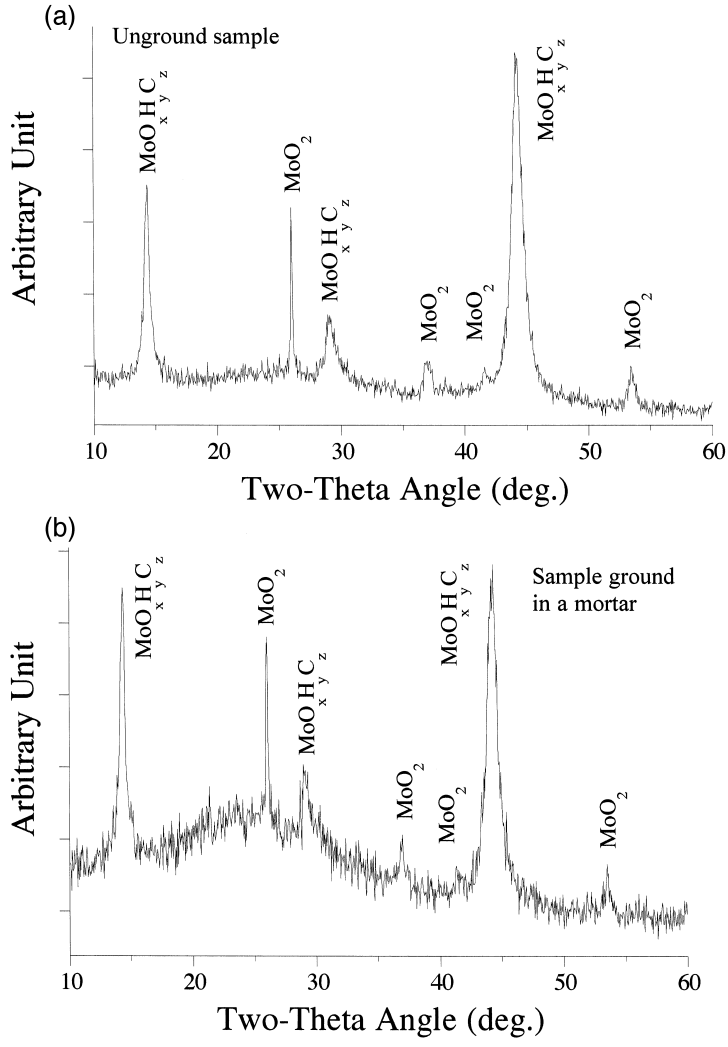

Fig. 4. XRD characterization of Mo-700 before and after grinding (a–b) after 3 h and (c–d) after 24 h activation.

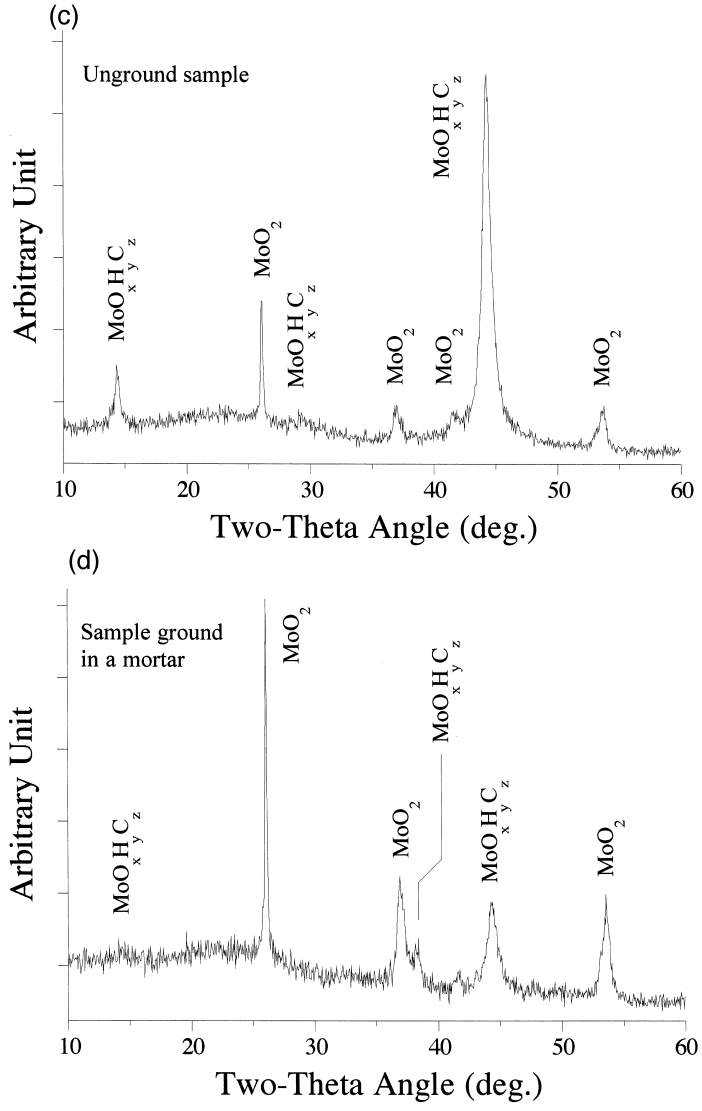

Fig. 4 (*continued*).

Table 1
Grinding effect on the relative intensity of the oxycarbide and MoO_2 diffraction peaks

Molybdenum oxycarbide			MoO_2		
2θ Angle	$I_{relative}$ before grinding	$I_{relative}$ after grinding	2θ Angle	$I_{relative}$ before grinding	$I_{relative}$ after grinding
38.00	0	60	26.05	100	100
44.20	100[a]	100	36.75[b]	63	54
64.20	0	15	53.60[b]	85	90

[a] The peak is always the strongest one, however, the absolute intensity was strongly decreased after grinding due to the destruction by grinding of the basal plane.

[b] XRD peak is composed by diffraction of several crystallographic plans with similar interreticular distances.

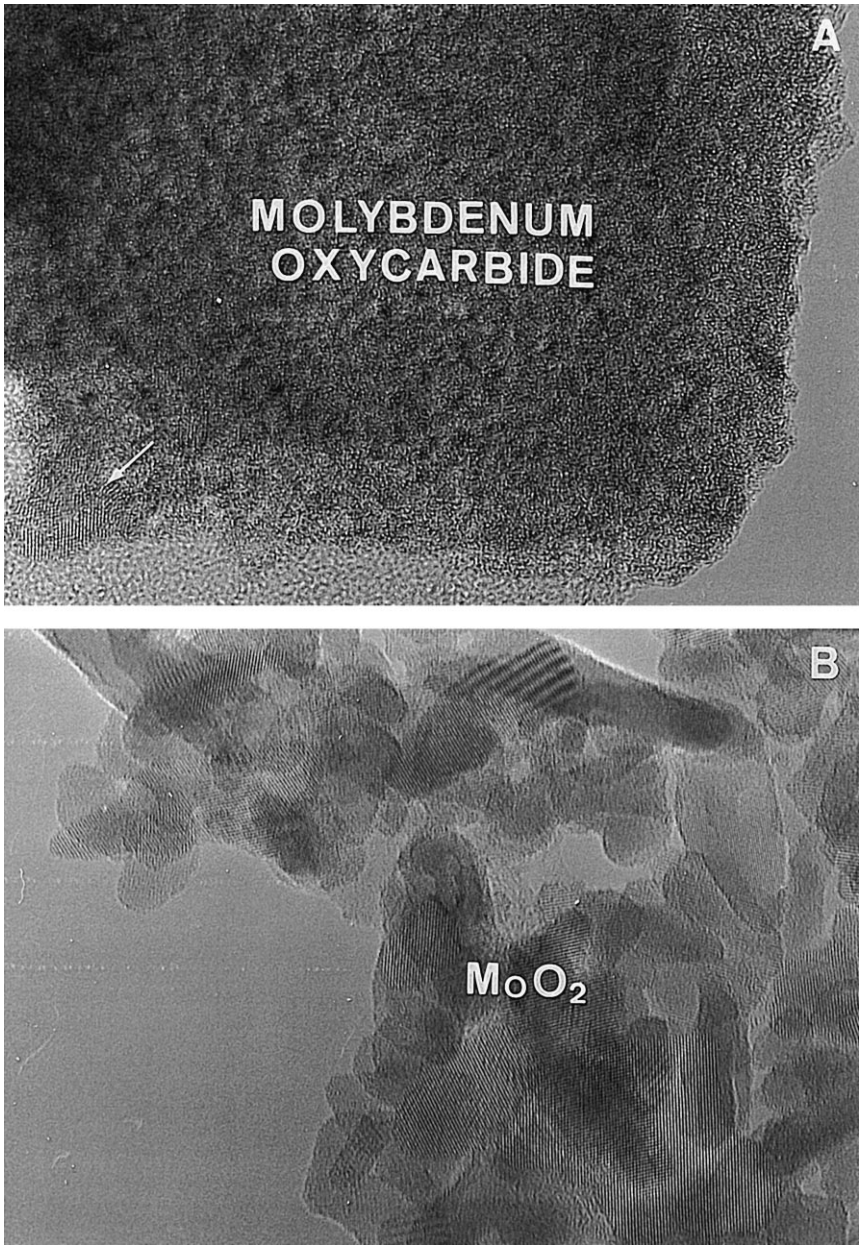

Fig. 5. TEM characterization of Mo-700 after 24 h activation. (a) TEM micrograph of molybdenum oxycarbide particle. According to SADP, all MoO_xC_y crystallites exhibit the same orientation. (b) High resolution micrograph of MoO_2. Oxide crystallites exhibit random orientation.

3.3. Activation under helium–n-heptane

XRD patterns of MoO_3 after 24 and 65 h time on stream are presented in Fig. 9. In the absence of hydrogen, the reduction of MoO_3 by *n*-C_7 led only to MoO_2, and no oxycarbide peaks were detected. The transformation process was much longer than with H_2/*n*-C_7 and MoO_3 was still present after 24

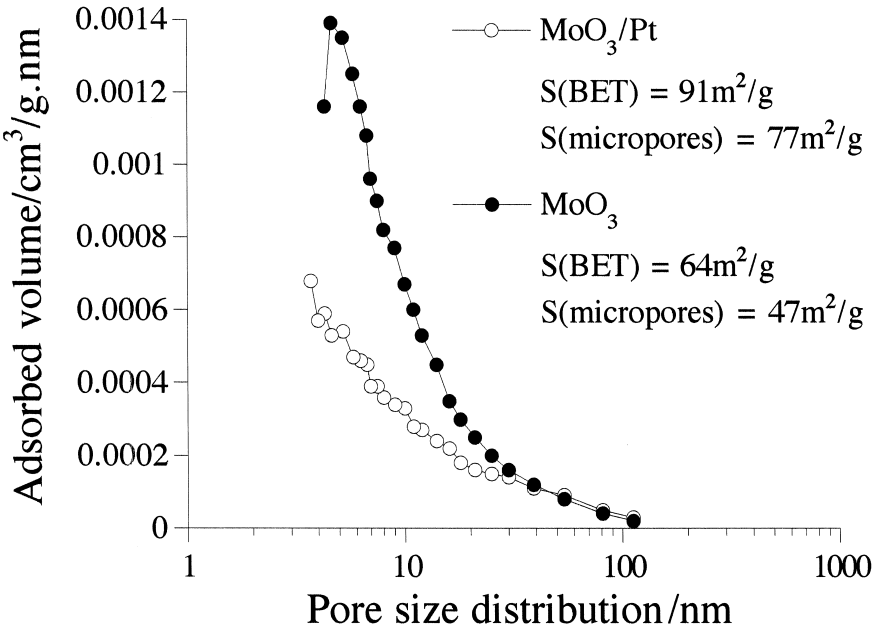

Fig. 6. Pore size distribution of molybdenum oxycarbohydride synthesized with and without platinum.

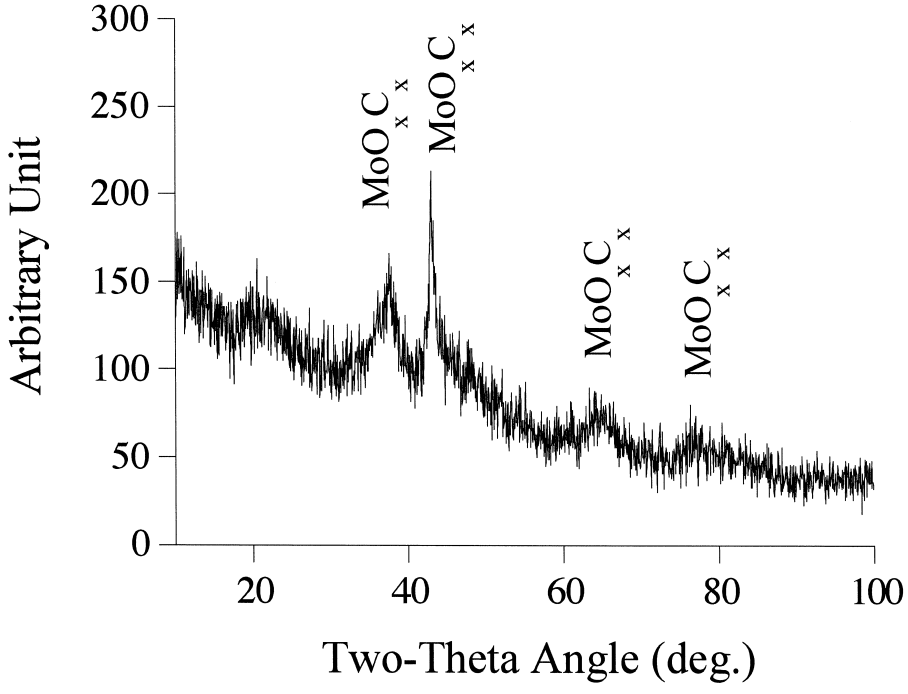

Fig. 7. XRD patterns of Mo–Pt after 24 h activation at 350°C and 7 bar total pressure. A pure oxycarbide phase has been formed.

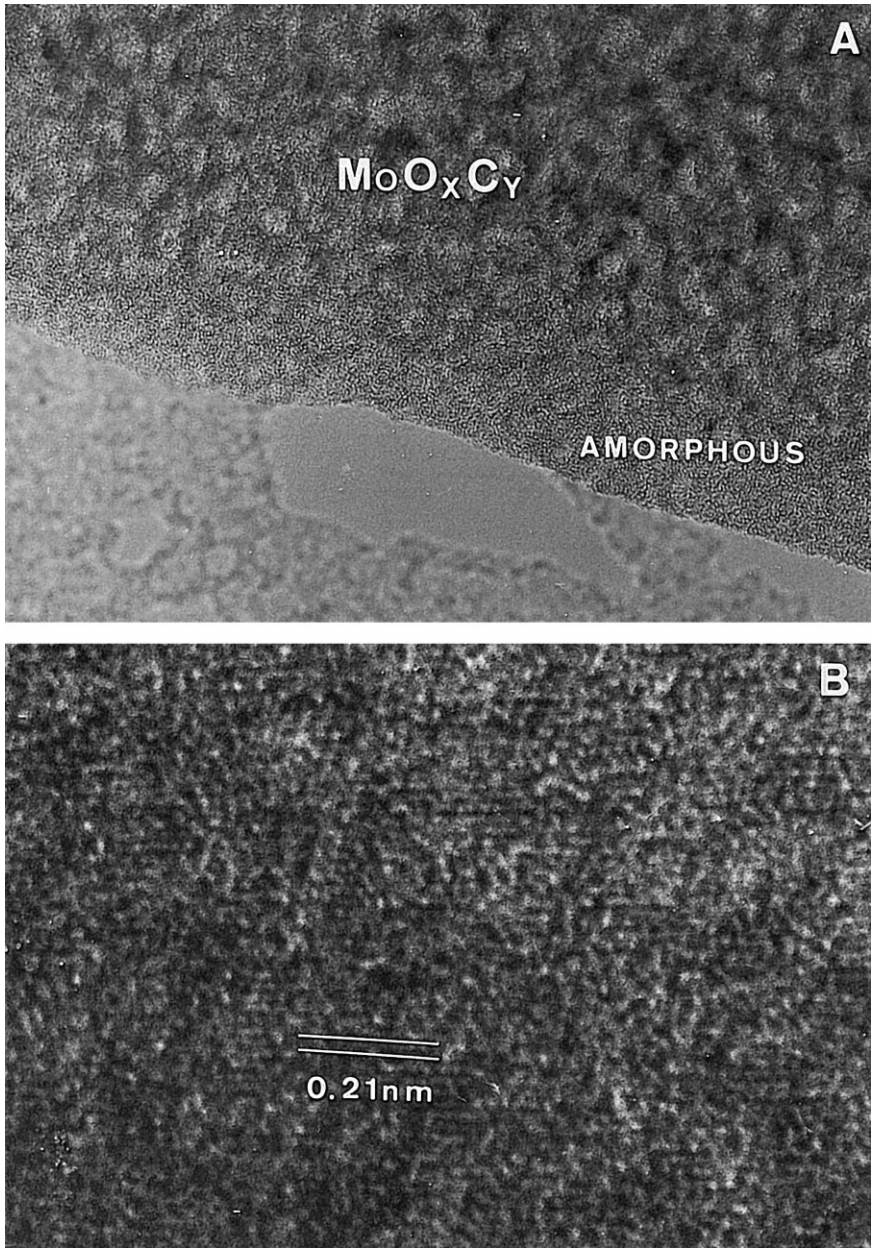

Fig. 8. TEM characterization of Mo–Pt after 24 h activation. (a) Micrograph of molybdenum oxycarbide particle. General aspects of the particle are very similar to the one previously observed on Mo-700. (b) High resolution micrograph of the particle, presence of crystallised nodule is evidenced.

h. This was attributed to the absence of hydrogen as main reductant.

HRTEM characterization of the solid after 65 h confirms that MoO_2 was the only phase formed (Fig. 10). Moreover, as confirmed by SADP, MoO_2 crystallites exhibited a random orientation, which was also consistent with a non-topotactic process (different orientations of the particles). No oxycarbide par-

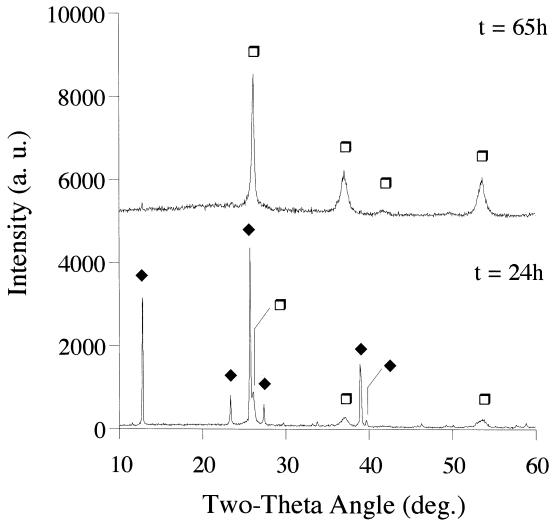

Fig. 9. XRD pattern of MoO_3 after (a) 24 and (b) 65 h under $He/n\text{-}C_7$ at 350°C. MoO_2 is the only phase detected.

ticles were evidenced in this sample. The presence of an amorphous phase was attributed to coke formation, as there was no hydrogen in the gaseous flow. Coke deposition also explained the difference between surface area deduced from the Scherrer method, 40 $m^2\ g^{-1}$, and from the BET method, 1 $m^2\ g^{-1}$. The MoO_2 particles were covered by a carbonaceous residue, which blocked the access of nitrogen to the oxide surface. Catalytic tests carried out on such samples show no evidence of isomerization activity.

3.4. Activation under pure hydrogen

XRD patterns of MoO_3 after 24 and 53 h time on stream are presented in Fig. 11. With pure hydrogen, the MoO_3 transformation led to two different compounds, MoO_2 and a compound iso-structural to the oxycarbide and so-called oxyhydride MoO_xH_y, previously reported by our group [27]. Both compounds were very stable with time on stream, as XRD patterns of the solid after 24 and 53 h were similar. It appeared that contrary to the absence of hydrogen, the alkane absence did not affect the structural transformation of MoO_3.

The transformation process was also accompanied by a strong development of the specific surface area and microporosity. After 24 h, S_{BET} was equal to 120 $m^2\ g^{-1}$, with a microporous surface area contribution as high as 75%.

4. Discussion

4.1. Hydrogen importance

It has been shown that the absence of hydrogen is detrimental to the oxycarbide synthesis, and MoO_2 is the only product formed. This is attributed to the crucial role of hydrogen, which does not only act as a classical reductant but also diffuses into the solid. In fact, the true precursors of the oxycarbide phase were molybdenum bronzes (H_xMoO_3) like compounds. This explains why with Mo–Pt as precursor, a pure oxycarbide phase can be synthesized, as it is well known that when Pt/MoO_3 is exposed to hydrogen, molybdenum bronzes are formed even at room temperature (hydrogen spillover) [28,29]. On the contrary, without platinum, part of the MoO_3 is reduced to MoO_2 before hydrogen has diffused into the solid. These observations are in good agreement with the work of Choi ett al. [18] and Jaggers et al. [19] who have shown that H_xMoO_3 are also precursors of the oxynitride phases. This also explains why MoO_2 cannot be a precursor to the oxycarbide or oxynitride phases [19], as this oxide cannot form molybdenum bronzes. Moreover, the hydrogen insertion in the solid is consistent with the elemental analysis results that always suggest the presence of hydrogen in the solid after synthesis. The catalyst should thus be better described as an oxycarbohydride $MoO_xH_yC_z$ rather than an oxycarbide MoO_xC_y.

In fact, in the absence of platinum, the MoO_2 presence may be of interest for the oxycarbide formation. Indeed, it is known that hydrogen can only diffuse in the atomic form (nascent hydrogen) into the solid [30]. This implies the formation at the surface of the solid of some active sites able to dissociate molecular hydrogen. It appears that MoO_2 itself may provide these sites, and as with Pt, addition of fresh MoO_2 to MoO_3 decreases the activation period [16]. Moreover, Sloczynski [31] reported that MoO_2 has a similar effect to platinum for the reduction of MoO_3 by hydrogen. Considering these facts, a proposed mechanism for the oxycarbide formation is shown in Fig. 12.

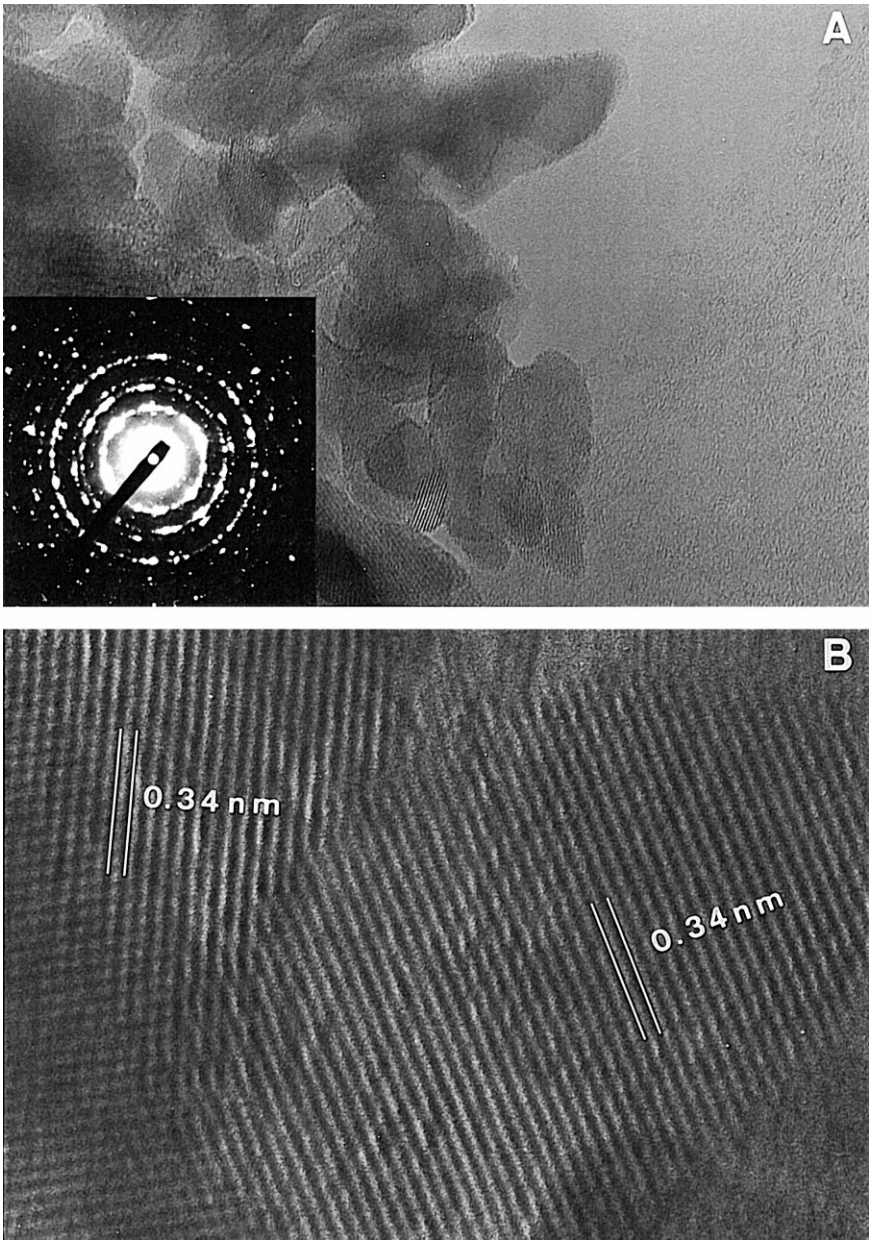

Fig. 10. TEM micrographs of MoO_3 after 24 h under He/*n*-C_7 at 350°C. (a) Low magnification image: MoO_2 crystallites exhibit random orientation, as confirmed by SADP, (b) High magnification image of MoO_2 crystallites and interplanar distance.

4.2. Nature of the transformation

The MoO_3–oxycarbide transformation is topotactic, with the (200) planes of $MoO_xH_yC_z$ parallel to the $(0k0)$ planes of the parent oxide. Considering the literature, the molybdenum oxynitride or oxycarbide formation seems to be directly linked to the topotaxy of the MoO_3 transformation under nitrating or carburising gaseous flow (Table 2).

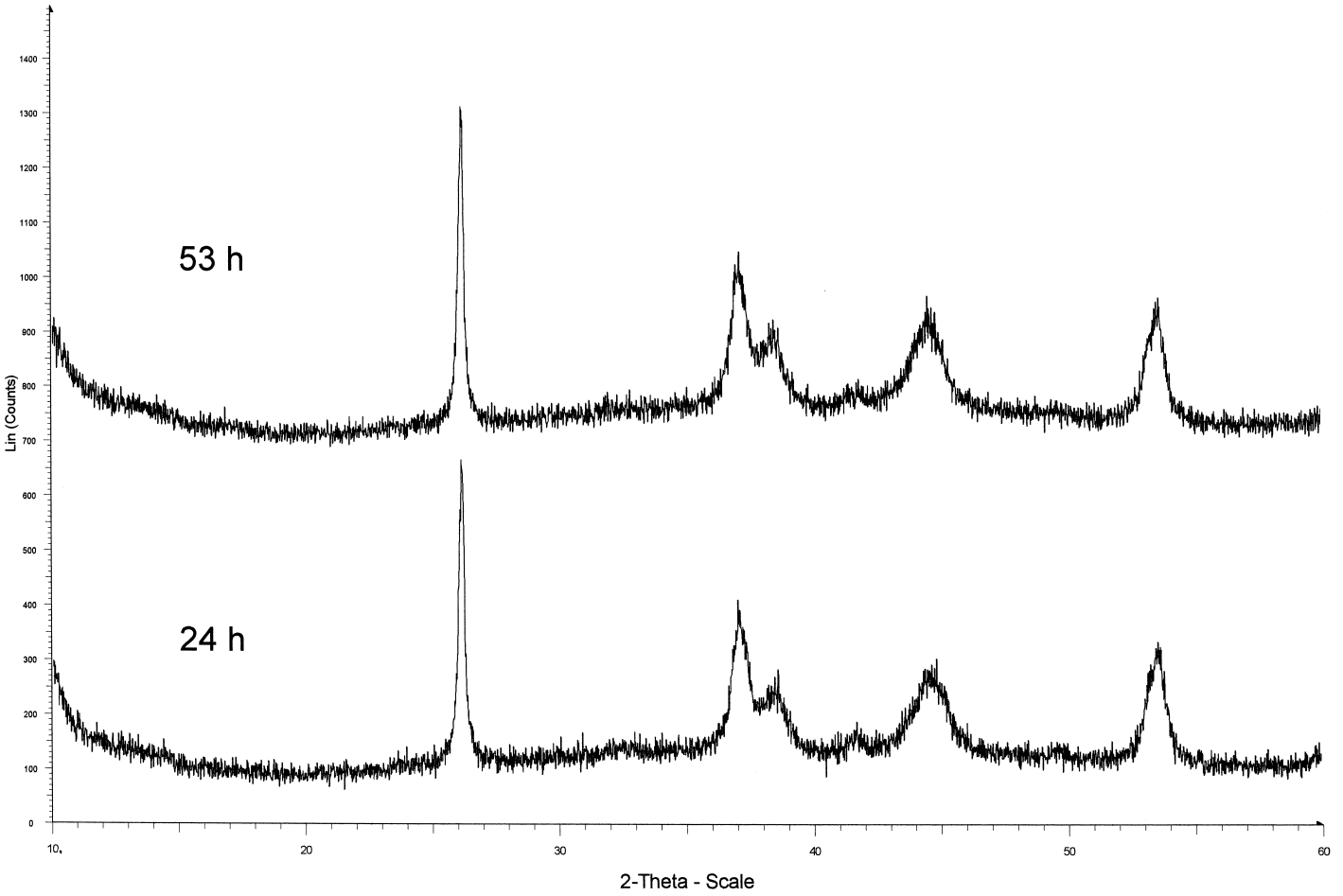

Fig. 11. XRD characterization of MoO_3 after (a) 24 and (b) 53 h reduction under pure hydrogen at 350°C. Formation of MoO_2 and MoO_xH_y is reported.

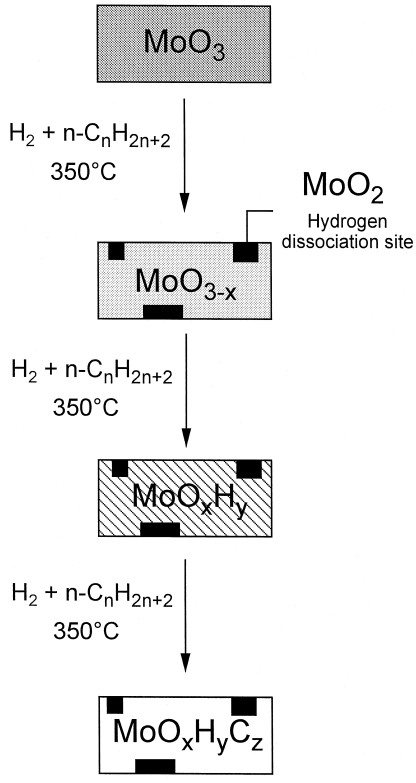

Fig. 12. Proposed mechanism for the oxycarbide phase formation in the absence of platinum. (1) Transformation of MoO_3 into MoO_{3-x} by hydrogen incorporation and reduction. (2) Formation of MoO_2 being then the active site for hydrogen dissociation. (3) Dissociated hydrogen over MoO_2 sites was subsequently incorporated into the MoO_3 phase to form the molybdenum oxyhydride. (4) Carbon incorporation into the molybdenum oxyhydride leading to the formation of the final molybdenum oxycarbohydride phase.

It is generally admitted that low temperature reactions are critical for the occurrence of topotactic transformation because a low temperature reaction imposes a restriction on displacement of the metallic atoms. This leads to an oriented nucleation of the product phase relative to the parent crystal [17]. Hydrogen diffusion in the solid is another critical parameter. Indeed, the 350°C reduction of MoO_3 with $He/n\text{-}C_7$ is non-topotactic, while at the same temperature MoO_3 reduction with $H_2/n\text{-}C_7$ turned out to be topotactic. In fact, it has been shown elsewhere [16] that TPR, under H_2 or H_2/methane, of H_xMoO_3 prepared without platinum leads to different intermediates and products than TPR of MoO_3 [16]. The hydrogen insertion strongly affects the reactivity of the solid towards a reducing or carburising gaseous flow.

The development of micropores, or small mesopores, also reflects the topotaxy of the transformation. During the topotaxy transformation the external shape of the solid was retained. As the external shape of the oxide particles is retained while the density between the starting product, oxide, and the final carbide was significantly modified, the solid develops voids between the small oxycarbide crystallites in order to accommodate such change and thus, leads to the formation of microporosity. We have shown elsewhere [16] that clean MoO_2 (without coke) synthesized by MoO_3 reduction does not develop any microporosity due to the fact that the transformation is not topotactic. It is also significant to note that metastable cubic $\alpha\text{-}MoC_{1-x}$ synthesized through a topotactic route develops high microporosity [17].

4.3. About Mo-700-3 h intermediate

The oxycarbide synthesis occurs through an intermediate phase not reported in the JCPDS files and

Table 2
MoO_3 nitruration or carburation: correlation between reaction products and topotactic reaction

	Nitruration		Carburization			
References	[18]	[34]	[17][a]	[32]	This work	This work[b]
Topotaxy process	Yes	Yes	Yes	No	Yes	No
Products	Oxynitride	Oxynitride	Oxycarbide	Without formation of oxycarbide	Oxycarbide	Without formation of oxycarbide
Surface area (m^2/g)	116	220	200	50–100	167	40

[a] With Pt (0.25 wt.%)/MoO_3 and in the presence of $H_2/n\text{-}C_7$.
[b] With $He/n\text{-}C_7$ instead of $H_2/n\text{-}C_7$.

called Mo-700-3 h. Considering crystallographic distances characteristic of this phase (i.e. 6.20, 3.05 and 2.05 Å) and the crystallographic structure of MoO_3, we propose that Mo-700-3 h is formed by contraction of the distance between the $(0k0)$ planes of MoO_3 (Fig. 13) and by a de-organization of the two-dimensional structure in the planes. The three crystallographic distances seen by XRD could correspond to first, second and third order diffraction of planes with a 6.20 Å interplanar distance.

This description of the intermediate phase well explains why the crystallographic direction of the $(0k0)$ planes is kept during the synthesis, and consequently why the reaction is topotactic. With time on stream, a further reorganization occurs in the amorphous planes, and the final fcc oxycarbide structure is formed (Fig. 13), with (200) planes parallel to the

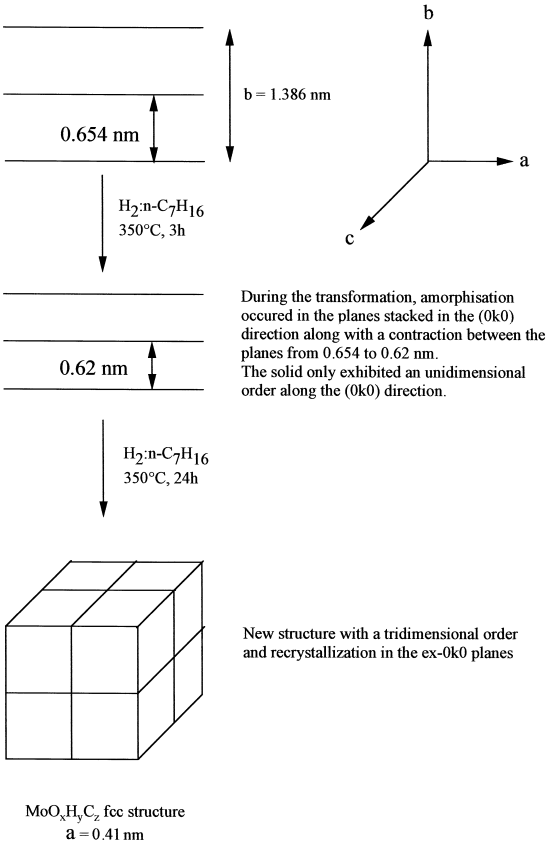

Fig. 13. Proposed description of the Mo-700-3 h intermediate formation. The intermediate structure directly derived from the contraction and amorphisation of the lamellar MoO_3 oxide.

initial $(0k0)$ MoO_3 planes. Mo-700-3 h can also be considered as a disorganized oxycarbide.

Interestingly, isostructural compounds have been reported in the literature, essentially for MoO_3 nitruration. Indeed, Lyutaya [33] reported the formation of an unknown intermediate MoO_2NH_2 (note the hydrogen presence) during MoO_3 nitruration by ammonia. Volpe [34] also reported the formation of a compound characterized by 6.15, 3.07 and 2.05 Å distances during the TPR of MoO_3 by ammonia. The compound was described as an oxynitride. Again, this observation shed light on the fact that hydrogen insertion is the key-point in the synthesis, regardless of the nature of the heteroatom (nitrogen with ammonia TPR, or carbon in our conditions). As proposed previously in Fig. 12, hydrogen insertion primarily dictates the structural transformation of MoO_3 to the intermediate compound. Then, depending on the nature of the gaseous flow, the solid can incorporate some C or N, and can be described as an oxycarbide or an oxynitride. The 350°C reduction of MoO_3 under pure hydrogen strongly supports this hypothesis, since even without any heteroatom, the same final fcc structure is formed, and a so-called MoO_xH_y oxyhydride is formed together with MoO_2. If a hydrocarbon is introduced, the oxyhydride will rapidly pick up some carbon to form, at least at the surface, the oxycarbide phase [16]. Oyama was the first to report a similar phenomenon for ammonia synthesis over catalyst based on Mo, Mo_2C and MoO_xC_y [35]. Djega-Mariadassou et al. [36] reported a similar result for propylbenzene hydrogenation with a molybdenum oxynitride catalyst. These authors reported that the superficial layer of the catalyst is carburized by the hydrocarbon and thus leads to the formation of a similar catalyst. More recently, Green et al. [37,38] also reported similar results for methane partial oxidation on molybdenum and tungsten carbide based catalysts and arrived to the same conclusion as above.

4.4. Catalytic properties of the solid formed with Mo-700 and Mo–Pt

Depending on the platinum presence, oxycarbides of different stoichiometry are formed: $MoO_{2.42}$-$C_{0.23}H_{0.75}$ with Mo-700 precursor, and $MoO_{0.91}$-

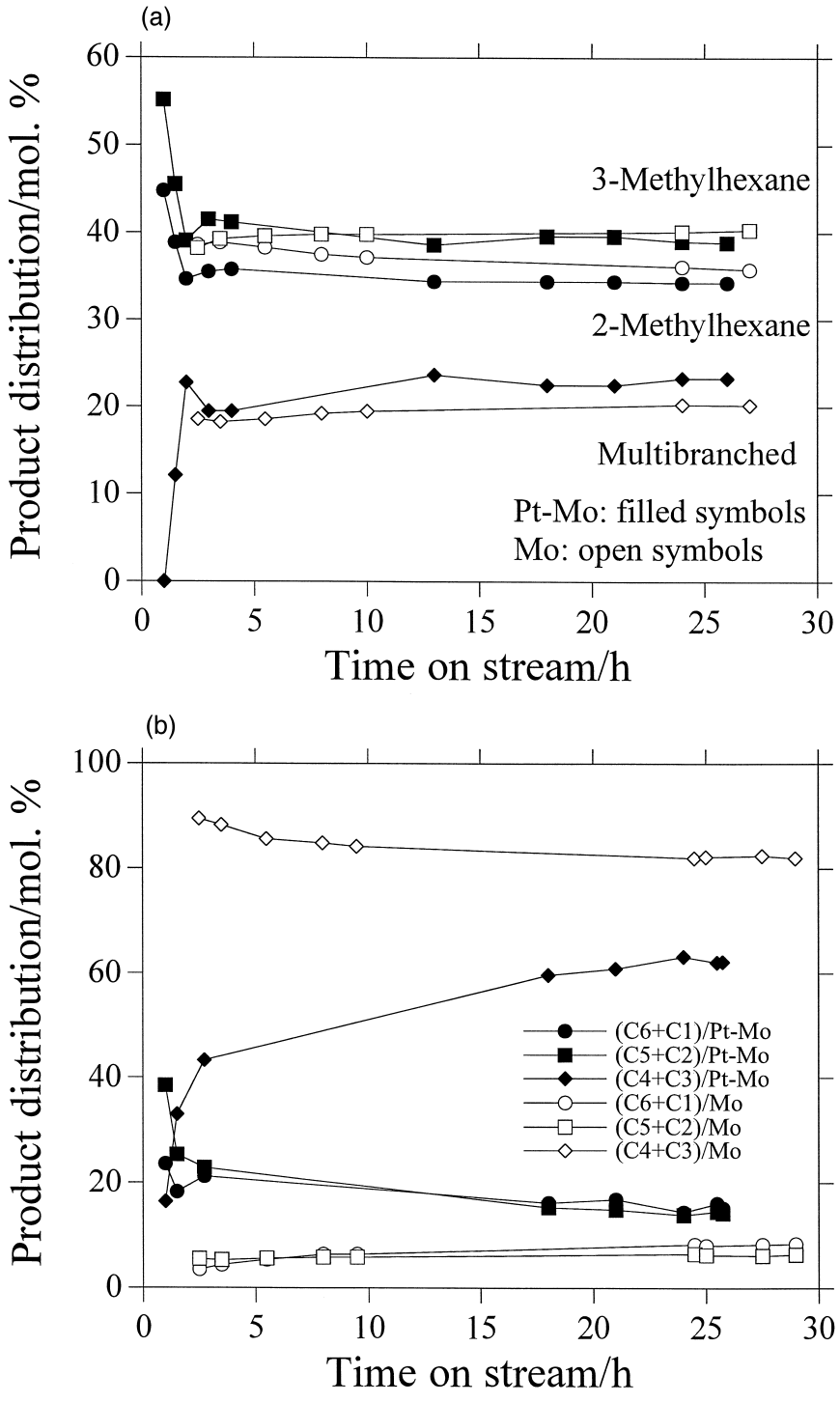

Fig. 14. (a) Comparison of isomers distribution on Mo-700 and Mo–Pt with time on stream. Comparison of cracking products distribution observed on Mo-700 and Mo–Pt with time on stream: (b) C_5/C_2 and multiple cracking, (c) C_4/C_3 and C_6/C_1.

$C_{0.49}H_{0.78}$ with Mo–Pt. A more carburized compound is obtained with platinum. The small a_{cub} increase (4.18 instead of 4.10 Å) also reflects the more carburised state of the oxycarbide synthesized in the presence of Pt [39]. Differences in the two oxycarbides stoichiometry can be attributed to the role played by platinum. In fact, Pt does not only allow H_xMoO_3 formation, but is also involved in the reduction–carburation process of the bronzes themselves, by activating the *n*-C_7 molecule. Lee et al. [17] have demonstrated that at a temperature as low as ca 250°C, Pt is able to activate methane molecules, producing carbon atoms that are incorporated into the solid to form molybdenum oxycarbide. One can easily understand that at 350°C and with *n*-C_7, which is more active than C_1, a similar phenomenon can occur.

It has been shown that the steady-state conversion and the isomerization selectivity on the two oxycarbides are very similar, which means that the two surfaces are nearly the same. This is also confirmed by close isomer distributions (Fig. 14a). The high amount of monobranched molecules is typical of an isomerization via a metallacyclobutane intermediate [40]. This similarity is not surprising, as both oxycarbides exhibit a fcc structure and contain O, C, and H. Note that comparison of product distributions is meaningful as both catalysts exhibit similar conversions at steady state.

However, small differences between the two catalysts are found if one considers the cracking product distributions (Fig. 14b). The multiple and end-chain crackings (C_5/C_2 and C_6/C_1) are more significant on the oxycarbide prepared with Mo–Pt. This phenomenon can be explained if one supposes that a difference in bulk composition also reflects a small difference in the surface composition. In this case, one expects the more carburised catalyst to exhibit a higher multiple cracking ability, as it is well known that pure carbides catalyse *n*-alkane hydrogenolysis [41]. The possible catalytic role of platinum is another possibility when explaining this phenomenon. Platinum particles can participate in *n*-C_7 multiple and end-chain cracking, thus increasing its contribution to cracking product distribution compared to oxycarbide without platinum. Moreover, this hypothesis explains the fact that at the very beginning of the Mo–Pt activation the catalyst exhibits a high multiple cracking ability. This should mainly be attributed to the catalytic properties of the platinum particles, as oxycarbide formation is not achieved.

5. Conclusion

The crucial role of hydrogen in the oxycarbide synthesis by MoO_3 reduction–carburation has been evidenced. It appeared that hydrogen diffusion into the solid to form bronze-like compounds was necessary for the oxycarbide synthesis. Dispersed platinum traces at the oxide surface was at the origin of the synthesis of a pure molybdenum oxycarbide phase, as Pt favoured hydrogen dissociation. Hydrogen allowed the MoO_3–oxycarbide formation to be topotactic, with the (200) oxycarbide planes parallel to the initial $(0k0)$ MoO_3 planes. In the absence of hydrogen, the transformation process turned out to be non-topotactic and only MoO_2 particles with different orientations were observed. Further publications will deal with the role of carbon for the synthesis of an active and selective isomerization catalyst.

Acknowledgements

The authors wish to thank Gaby Ehret (Groupe Surface-Interface, Institut de Physique et Chimie des Matériaux de Strasbourg, UMR 7504 CNRS) for TEM experiments. Dr. Baudouin Heinrich (ONERA, DEFA, Châtillon, France) is also gratefully acknowledged for helpful discussions during this work.

References

[1] J.L. Nocca, A. Forestiere, J. Cosyns, Rev. Inst. Fr. Pet. 49 (1994) 461.
[2] M. Steijns, G.F. Froment, P. Jacobs, P. Uytterhoven, J. Weitkamp, Ind. Eng. Prod. Res. Dev. 20 (1981) 654.
[3] J.M. Campelo, F. Lafont, M. Marinas, J. Catal. 156 (1995) 11.
[4] S.M. Jacob, F.X. Banta, T.M. Hoo, M.P. McGuiness, R.J. Quann, E. Sanchez, P.O. Staffeld, M.E. Wells, R.G. Wuest, Paper No. 25c, AIChE 1998 Spring National Meeting.
[5] R.J. Taylor, R.H. Petty, Appl. Catal. A 119 (1994) 121.
[6] M. Belloum, C. Travers, J.P. Bournonville, Rev. Inst. Fr. Pet. 46 (1991) 89.

[7] I. Wang, Y.J. Chang, Stud. Surf. Sci. Catal. 92 (1995) 155.
[8] J. Weitkamp, ACS symposium, Am. Chem. Soc. (1975) 1.
[9] M.J. Ledoux, J. Guille, C. Pham-Huu, H.M. Dunlop, M. Prin, US Patent No. 5 468 370 (1990), assigned to Pechiney Recherche.
[10] E.A. Blekkan, C. Pham-Huu, M.J. Ledoux, J. Guille, Ind. Eng. Chem. Res. 33 (1994) 1657.
[11] C. Pham-Huu, P. Del Gallo, E. Peschiera, M.J. Ledoux, Appl. Catal. A 132 (1995) 77.
[12] P. Delporte, C. Pham-Huu, M.J. Ledoux, Appl. Catal. A 149 (1997) 151.
[13] M.J. Ledoux, S. Roy, C. Pham-Huu, C. Crouzet, C. Bouchy, Proc. AIChE (1998) 201.
[14] M.J. Ledoux, S. Roy, C. Bouchy, C. Pham-Huu, Proc. AIChE (1998) New Orleans.
[15] C. Bouchy, C. Pham-Huu, B. Heinrich, C. Chaumont, M.J. Ledoux, J. Catal. 190 (2000) 92.
[16] C. Bouchy, PhD Dissertation, Strasbourg University (1998).
[17] J.S. Lee, L. Volpe, F.H. Ribeiro, M. Boudart, J. Catal. 112 (1988) 44.
[18] J.G. Choi, R.L. Curl, L.T. Thompson, J. Catal. 146 (1994) 218.
[19] C.H. Jaggers, J.N. Michaels, A.M. Stacy, Chem. Mater. 2 (1990) 150.
[20] H.C. Zeng, C.W. Sheu, H.C. Hia, Chem. Mater. 10 (1998) 974.
[21] J.H. de Boer, in: D.H. Everett (Ed.), The Structure and Properties of Porous Materials, 1958.
[22] A.P.E. York, C. Pham-Huu, P. Del Gallo, E.A. Blekkan, M.J. Ledoux, Ind. Eng. Chem. Res. 35 (1996) 672.
[23] C. Pham-Huu, A.P.E. York, M. Benaissa, P. del Gallo, M.J. Ledoux, Ind. Eng. Chem. Res. 34 (1994) 1107.
[24] Compound identified by comparison with the JCPDS file n 32.0671.
[25] H.R. Oswald, J.R. Gunter, in: E. Kaldis, H.J. Scheel (Eds.), Crystals Growth and Materials, 1977.
[26] X. Gouin, PhD Dissertation, Rennes University (1993).
[27] P. Delporte, F. Meunier, C. Pham-Huu, P. Venneges, M.J. Ledoux, J. Guille, Catal. Today 23 (1995) 251.
[28] R. Erre, H. Van Damme, J.J. Fripiat, Surf. Sci. 127 (1983) 48.
[29] R. Benali, C. Hoang-Van, P. Vergnon, Bull. Soc. Chim. Fr. 3 (1985) 417.
[30] D. Tinet, J.J. Fripiat, J. Chim. Phys. 76 (10) (1979) 867.
[31] J. Sloczynski, J. Solid State Chem. 118 (1995) 84.
[32] J.S. Lee, S.T. Oyama, M. Boudart, J. Catal. 106 (1987) 125.
[33] M.D. Lyutaya, Sov. Powder Metall. Met. Ceram. 3 (1979) 190.
[34] L. Volpe, PhD Dissetation, Stanford University (1985).
[35] S.T. Oyama, PhD Dissertation, Stanford University (1981).
[36] G. Djega-Mariadassou, M. Boudart, G. Bugli, C. Sayag, Catal. Lett. 31 (1995) 411.
[37] A.P.E. York, J.B. Claridge, A.J. Brungs, S.C. Tsang, M.L.H. Green, Chem. Commun. (1997) 39.
[38] J.B. Claridge, A.P.E. York, A.J. Brungs, C. Marquez-Alvares, J. Sloan, S.C. Tsang, M.L.H. Green, J. Catal. 180 (1998) 85.
[39] E.K. Storms, Refractory Carbides, Academic Press, New York, 1967.
[40] C. Pham-Huu, M.J. Ledoux, J. Guille, J. Catal. 143 (1993) 249.
[41] E. Iglesia, F.H. Ribeiro, M. Boudart, J.E. Baumgartner, Catal. Today 15 (1992) 307.